Bulletin of the Institute of Mathematics
Academia Sinica (New Series)
Vol. **3** (2008), No. 4, pp. 469-486

PHASE DYNAMICS FOR NONLINEAR DISSIPATIVE WAVES UNDER EXTERNAL AND FEEDBACK CONTROL

BY

TAKAO OHTA

Abstract

We study dynamics of traveling waves under spatio-temporal forcing in non-equilibrium systems. Based on the model equations of nonlinear dissipative systems where traveling waves are formed in a self-organized manner, we apply external and feedback forcing to the traveling waves. Entrainment and modulation of the traveling waves are investigated numerically and analytically in one dimension. In the present paper, we focus our attention on the trapped oscillations of the waves under the external forcing and the propagation reversal in the feedback forcing. A phase dynamic approach is developed to formulate these interesting and unexpected dynamics.

1. Introduction

Self-organized formation of spatio-temporal patterns far from equilibrium has been studied extensively both experimentally and theoretically for many years [1]. Among the various model systems, a set of reaction diffusion equations has been shown to be very useful to explore pattern evolution in numerical simulations and to develop theories as Mimura and his coworkers have made important contributions for these three decades [2].

One of the most recent topics is to control these nonequilibrium patterns by external forcing. Because the system is far from equilibrium, the

Received Auguest 12, 2008.

response itself is generally nonlinear and often interesting unexpected dynamics emerge. A well-known example is synchronization of oscillators with the external periodic perturbation [3]. More complex examples are photo-induced waves in liquid-crystalline monolayers [4, 5, 6], convective nematic fluid under spatially periodic forcing [7] and influence of external modulation in convective fluids [9] and in chemical reactions [10, 11, 12].

Another procedure to control nonequilibrium patterns is to feedback the information of the system, which is intrinsically nonlinear. Such control would be useful to stabilize some pattern which would be unstable in the absence of the feedback and has potential applications in a wide range of fields, from material sciences to biology [13, 14]. It has been demonstrated in a simple oscillating system without spatial degrees of freedom that the dynamics subjected to a feedback-mediated control possess many common features [15, 16]. It is also mentioned that extension to spatially nonuniform control has been attempted recently [17, 18, 19, 20, 21, 22].

Quite recently we have studied external and feedback forcing in nonlinear dissipative propagating waves in one dimension [23, 24, 25]. The dynamics have been investigated in details by changing the magnitudes and other parameters of the forcing. Here, we focus our attention on two interesting phenomena which appear only in propagating waves. One is trapped coherent oscillations of waves for static spatially periodic forcing. The other is a reversal of the propagating direction when the waves are subjected to feedback forcing. The theory in terms of a coupled set of phase variables has also been developed to understand these interesting dynamics.

The organization of the present paper is as follows. In the next section, we start with a brief explanation of the model system and the linear stability analysis of the uniform equilibrium solution. In Section 3, we describe the trapped oscillation subjected to static forcing and its theoretical analysis in terms of the phase dynamcis. In Section 4. we show the numerical simulations of the propagating reversal under feedback forcing. The phase dynamics approach to this phenomenon is formulated in Section 5. Discussion is given in Section 6.

2. Model Equation and Linear Stability

As a model system for nonlinear dissipative waves, we consider phase separation undergoing chemical reactions [26, 27, 28]. This hypothetical mixture is composed of three chemical components A, B and C which undergo a cyclic chemical reaction

$$A \to B \to C \to A \tag{1}$$

with the reaction rates γ_1 from A to B, γ_2 from B to C and γ_3 from C to A. We assume that there are other components involved in the chemical reaction, which are supplied to the system and removed from the system sufficiently rapidly so that they are constant in both space and time and their effects are absorbed into the reaction rates.

We suppose that A and B species tend to segregate each other whereas the component C is neutral for both A and B and is not diffusive. The simplest time-evolution equations which take account of the chemical reactions and the phase separation are given by [26]

$$\frac{\partial \psi}{\partial t} = \nabla^2 \frac{\delta F}{\delta \psi} + f(\psi, \phi), \tag{2}$$

$$\frac{\partial \phi}{\partial t} = g(\psi, \phi), \tag{3}$$

with $\psi = \psi_A - \psi_B$ and $\phi = \psi_A + \psi_B$, where ψ_A, ψ_B and ψ_C denote the local concentrations of A, B and C components respectively. We have imposed the condition $\psi_A + \psi_B + \psi_C = 1$ which is justified by the assumption of the uniformity of other chemical species as mentioned above. The free energy functional F is given by

$$F = \int d\mathbf{r} \left[\frac{D}{2} (\nabla \psi)^2 - \frac{\tau}{2} \psi^2 + \frac{1}{4} \psi^4 \right], \tag{4}$$

where D and τ are positive constants. The last terms in eqs. (2) and (3) arise from the chemical reaction (1) and are given, respectively, by

$$f(\psi, \phi) = -\left(\gamma_1 + \frac{\gamma_2}{2}\right) \psi - \left(\gamma_1 - \frac{\gamma_2}{2} + \gamma_3\right) \phi + \gamma_3, \tag{5}$$

$$g(\psi, \phi) = \frac{\gamma_2}{2} \psi - \left(\frac{\gamma_2}{2} + \gamma_3\right) \phi + \gamma_3. \tag{6}$$

The uniform stationary solution of eqs. (2) and (3) are readily obtained as

$$\psi_0 = \frac{\gamma_3(\gamma_2 - \gamma_1)}{\gamma_1\gamma_2 + \gamma_2\gamma_3 + \gamma_3\gamma_1}, \tag{7}$$

$$\phi_0 = \frac{\gamma_3(\gamma_2 + \gamma_1)}{\gamma_1\gamma_2 + \gamma_2\gamma_3 + \gamma_3\gamma_1}. \tag{8}$$

We study the linear stability of the uniform solution putting $\psi - \psi_0 = c_1 \exp(\lambda t + iqx)$ and $\phi - \phi_0 = c_2 \exp(\lambda t + iqx)$ with c_1 and c_2 constants. In this section, we fix the parameters as $D = 1$, $\gamma_1 = 0.3$ and $\gamma_3 = 0.05$ and the remaining two parameters τ and γ_2 are varied. At some range of the parameters, the eigenvalue λ is complex. An example is shown in Figure 1 (a) for $\tau = 1.46$ and $\gamma_2 = 0.16$. Note that the real part is close to zero at a finite wave number q_c and the imaginary part has a minimum at $q = q_c$. The latter is a general property of the present model system. If we choose a slightly larger value of τ fixing other parameters, the real part becomes positive in the vicinity of $q = q_c$. The expressions of q_c, τ_c and the critical frequency ω_c which is the imaginary part of the eigenvalue at $q = q_c$ are given for $\tau > 3\psi_0^2$ by

$$q_c = \left(\frac{\tau - 3{\psi_0}^2}{2}\right)^{1/2}, \tag{9}$$

$$\tau_c = 3{\psi_0}^2 + 2(\gamma_1 + \gamma_2 + \gamma_3)^{1/2}, \tag{10}$$

$$\omega_c = \left(\frac{\gamma_1\gamma_2 - \gamma_2\gamma_3 - {\gamma_2}^2}{2} - {\gamma_3}^2\right)^{1/2}. \tag{11}$$

The bifurcation diagram obtained by the linear stability analysis is depicted in Figure 1 (b) [27]. Numerical simulations of eqs. (2) and (3) in one dimension show that a motionless periodic pattern appears in the region indicated by $\times$ in Figure 1 (b) whereas a propagating wave pattern appears in the region $+$. The Euler method is employed with the system size $L = 64$, the mesh size 0.5 and the time increment 0.001 and a periodic boundary condition is imposed. The value of τ at the Hopf bifurcation point for $\gamma_2 = 0.16$ is $\tau_c \approx 1.46$ at which the critical wave number is $q_c \approx 0.9$ and the critical frequency $\omega_c \approx 0.07$.

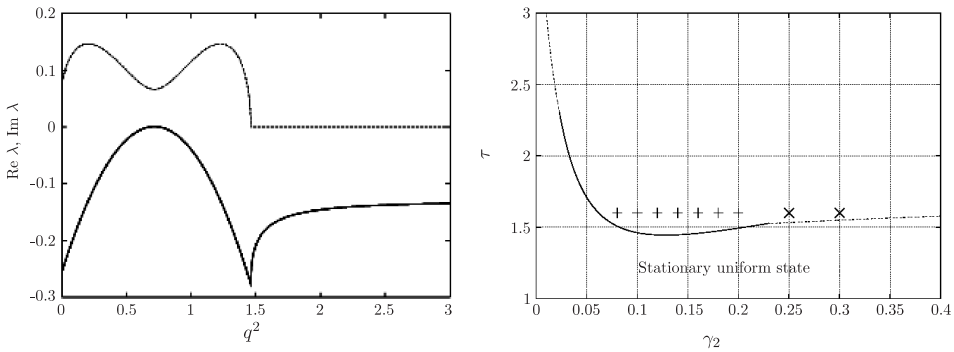

Figure 1. (a) The wave-number dependence of Re $\lambda(q)$ (solid curve) and Im $\lambda(q)$ (dashed curve) for $D = 1.0$, $\tau = 1.46$, $\gamma_1 = 0.3$, $\gamma_2 = 0.16$ and $\gamma_3 = 0.05$. The vertical and horizontal axes are dimensionless. (b) Bifurcation diagram for the uniform stationary solution for $D = 1$, $\gamma_1 = 0.3$ and $\gamma_3 = 0.05$. The full curve and the dotted curve are the Hopf bifurcation line and the Turing-type bifurcation line respectively. A traveling wave appears at the parameters indicated by the symbol + whereas a motionless pattern at the symbol $\times$.

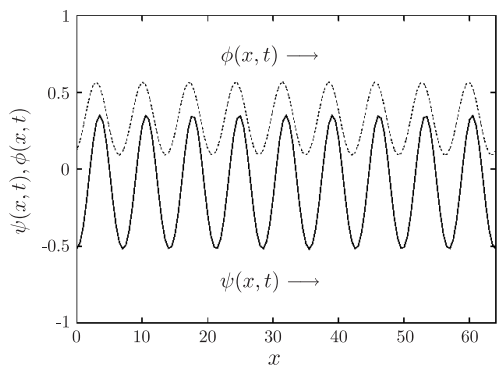

Figure 2. Spatial profiles of $\psi(x,t)$ (solid curve) and $\phi(x,t)$ (dashed curve) for $D = 1.0, \tau = 1.6, \gamma_1 = 0.3, \gamma_2 = 0.16$ and $\gamma_3 = 0.05$. Both $\psi(x,t)$ and $\phi(x,t)$ are propagating to the right at the same velocity.

Figure 2 shows an example of the propagating wave. Since eqs. (2) and (3) are invariant under the transformation $x \to -x$, the traveling wave can propagate either to the right or to the left with the proper phase difference between ϕ and ψ. Hereafter we choose (with an appropriate initial condition) a wave traveling to the right without loss of generality.

3. Trapped Oscillation by the External Forcing

In order to investigate the modulation of the traveling waves under external forcing, we add a new term to eqs. (2) and (3)

$$\Gamma(x,t) = \epsilon \cos(q_f x) \tag{12}$$

where ϵ is the magnitude of the forcing and $2\pi/q_f$ is the spatial period. Throughout this paper, we restrict ourselves to the case that the spatial period of the traveling wave is the same as $2\pi/q_f$, i.e., $q_c = q_f$. The parameters are chosen such that the system is near the bifurcation threshold so that the spatio-temporal dependence of the wave is not much deviated from a sinusoidal function. The model equations (2) and (3) are modified as

$$\frac{\partial \psi}{\partial t} = \nabla^2 \left[-\nabla^2 \psi - \tau\psi + \psi^3\right] + a_1\psi + a_2\phi + \epsilon\cos(q_f x) + a_3, \tag{13}$$

$$\frac{\partial \phi}{\partial t} = b_1\psi + b_2\phi + \epsilon\cos(q_f x) + b_3, \tag{14}$$

where

$$a_1 = -\left(\gamma_1 + \tfrac{\gamma_2}{2}\right), \quad a_2 = -\left(\gamma_1 - \tfrac{\gamma_2}{2} + \gamma_3\right), \quad a_3 = \gamma_3,$$
$$b_1 = \tfrac{\gamma_2}{2}, \quad b_2 = -\left(\tfrac{\gamma_2}{2} + \gamma_3\right), \quad b_3 = \gamma_3.$$

Equations (13) and (14) are solved numerically [23]. When the strength of the external forcing ϵ is small, the amplitude and the velocity of the wave are modulated periodically. The space-time plot of ψ in this case is displayed

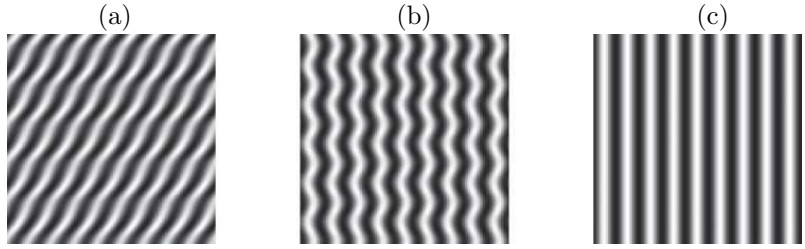

Figure 3. Space (horizontal) -time (vertical) plot of ψ for (a) $\epsilon = 0.005$, (b) $\epsilon = 0.01$ and (c) $\epsilon = 0.02$. The parameters are chosen as $\tau = 1.6$ and $\gamma_2 = 0.16$. The gray scale indicates the magnitudes of ψ.

in Figure 3(a). However, beyond a certain critical value $\epsilon = {\epsilon_1}^* \approx 0.0055$ for $\tau = 1.6$ and $\gamma_2 = 0.16$, the waves cannot propagate any more but undergo a coherent oscillation trapped by the external force as shown in Figure 3(b). There is another threshold at $\epsilon = {\epsilon_2}^* \approx 0.0141$ above which the waves do not move but they are pinned as is evident in Figure 3(c).

We shall show that these two bifurcations can be understood by a phase dynamics approach [25]. What we examine here is the stability of the stationary (pinned) solution for sufficiently large values of ϵ. We put

$$\psi = \psi_0 + \psi_1 \cos(q_c x), \tag{15}$$

$$\phi = \phi_0 + \phi_1 \cos(q_c x). \tag{16}$$

We have verified that the harmonic variation of ψ and ϕ is a good approximant of the simulation results. Numerical simulations indicate that the spatial variation of ψ and ϕ is anit-phase with respect to the external spatial modulation $\epsilon \cos(q_c x)$. Therefore both ψ_1 and ϕ_1 are negative.

Substituting (15) and (16) into (13) and (14) and ignoring higher harmonics, we obtain

$$-{q_f}^4\psi_1 + \tau {q_f}^2\psi_1 - {q_f}^2(3\psi_0^2\psi_1 + \frac{3}{4}\psi_1^3) + a_1\psi_1 + a_2\phi_1 + \epsilon = 0, \tag{17}$$

$$b_1\psi_1 + b_2\phi_1 + \epsilon = 0. \tag{18}$$

This gives us the amplitudes of the motionless periodic solutions $\psi_1 = \bar{\psi_1}(\leq 0)$ and $\phi_1 = \bar{\phi_1}(\leq 0)$. In order to study the stability of this pinned solution, we introduce the time-dependent phase variables as

$$\psi = \psi_0 + \bar{\psi_1} \cos q_c(x + \theta_1(t)), \tag{19}$$

$$\phi = \phi_0 + \bar{\phi_1} \cos q_c(x + \theta_2(t)). \tag{20}$$

Substituting (19) and (20) into (13) and (14) and multiplying the resultant equations, respectively, by $\sin q_c(x + \theta_1(t))$ and $\sin q_c(x + \theta_2(t))$, and performing the integral over x, we obtain

$$q_c \frac{d\theta_1}{dt} = c_{11} \sin q_c(\theta_1 - \theta_2) + c_{12} \sin(q_c\theta_1), \tag{21}$$

$$q_c \frac{d\theta_2}{dt} = -c_{21} \sin q_c(\theta_2 - \theta_1) + c_{22} \sin(q_c\theta_2), \tag{22}$$

where

$$c_{11} = -\frac{a_2\bar{\phi}_1}{\bar{\psi}_1}, \quad c_{12} = -\frac{\epsilon}{\bar{\psi}_1}, \\ c_{21} = \frac{b_1\bar{\psi}_1}{\bar{\phi}_1}, \quad c_{22} = -\frac{\epsilon}{\bar{\phi}_1}. \tag{23}$$

It is noted that these coefficients are positive. Linearizing the set of eqs. (21) and (22) around the stationary solution $\theta_1 = \theta_2 = 0$, we obtain the eigenvalue equation

$$\lambda^2 - (c_{11} + c_{12} - c_{21} + c_{22})\lambda + c_{11}c_{22} - c_{21}c_{12} + c_{12}c_{22} = 0. \tag{24}$$

The Hopf instability condition is given by

$$c_{11} + c_{12} - c_{21} + c_{22} \ > \ 0, \tag{25}$$

and

$$c_{11}c_{22} - c_{21}c_{12} + c_{12}c_{22} \ > \ 0. \tag{26}$$

We have verified numerically that the condition (26) is always satisfied. The condition (25) yields ${\epsilon_2}^* = 0.01404$ which agrees quite well with the bifurcation point ${\epsilon_2}^* = 0.0141$ obtained by numerical simulations. For $\epsilon < {\epsilon_2}^*$, the set of equations (21) and (22) exhibits a limit cycle oscillation as shown in Figure 4(a). The oscillations themselves of ψ and ϕ are found to be quantitatively in agreement with the simulations (though not shown).

If the value of ϵ is further decreased, the limit cycle oscillation disappears

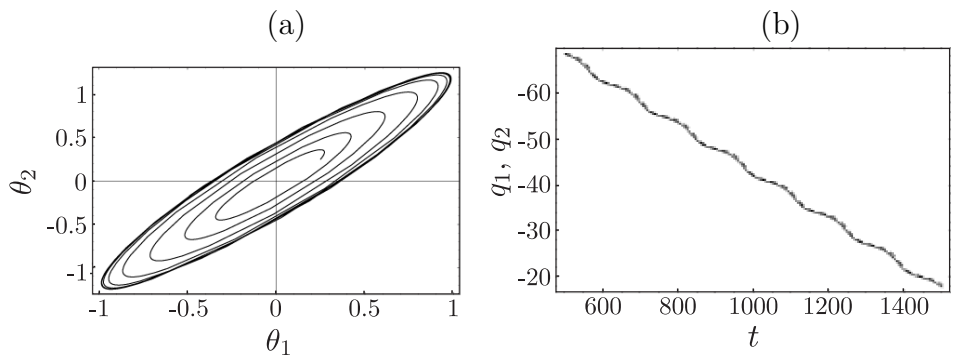

Figure 4. (a) Limit cycle oscillation of θ_1 and θ_2 for $\epsilon = 0.01$. (b) Time-evolution of θ_1 (solid curve) and θ_2 (dashed curve) for $\epsilon = 0.004$.

in eqs. (21) and (22) and it turns out that θ_1 and θ_2 increase (or decrease) monotonously as shown in Figure 4 (b). This behavior corresponds to the modulated traveling wave displayed in Figure 3(a) and occurs for ϵ smaller than $\epsilon \approx 0.0044$ which is slightly smaller than the other bifurcation threshold $\epsilon_1^* = 0.0055$ obtained numerically. This discrepancy is attributed to the fact that the approximation used in the derivation of eqs. (21) and (22), which are valid around the pinned solution, becomes worse for smaller values of ϵ. Nevertheless, the theory reproduces the simulations qualitatively and the global dynamics are understood almost completely [25].

4. Feedback control

The feedback effect of the propagating waves is investigated by using the equations

$$\frac{\partial \psi}{\partial t} = \nabla^2 \left[-\nabla^2 \psi - \tau \psi + \psi^3\right] + a_1 \psi + a_2 \phi + a_3 + F[\psi(x-\delta, t) - \bar{\psi}], \quad (27)$$

$$\frac{\partial \phi}{\partial t} = b_1 \psi + b_2 \phi + b_3 + F[\psi(x-\delta, t) - \bar{\psi}], \quad (28)$$

where the coefficient F is the strength of the feedback term and $\bar{\psi}$ is the spatial average of ψ. (This should not be confused with $\bar{\psi}$ in eq. (19).) Note that we have added a term given by the profile of ψ but with a space shift δ. We examine how the propagating waves are affected by the feedback term by changing the strength F and the spatial shift δ [25].

As mentioned in Section 1, our main purpose is to investigate the dynamics of traveling waves under feedback-mediated spatio-temporal control in distributed systems. In the previous studies of such feedback control, time-delayed feedback was employed to derive a well-defined relationship between the external frequency Ω and the phase difference between the external force and the entrained oscillations [3]. In eqs. (27) and (28), by contrast, we have employed a spatially shifted control. Note that, in contrast to the time-delay control, such a spatial shift can be either positive or negative. Another reason that we employ this type of control is that it is easily treated both numerically and analytically. Some unexpected interesting dynamics appear as will be shown below.

We have solved eqs. (27) and (28) numerically in one dimension [25]. Initially, we start with the set of equations with $F = 0$. After a wave propagating to the right has developed, we turn on the feedback term, setting F to some finite value. The asymptotic traveling velocity V is evaluated as a function of the spatial shift δ for a given value of F. The relation between the frequency $\Omega_{FB} = q_c V$ of the controlled wave and the normalized phase shift $\Delta = q_c\delta/2\pi$ is displayed in Figures 5(a)-(d) for four values of F.

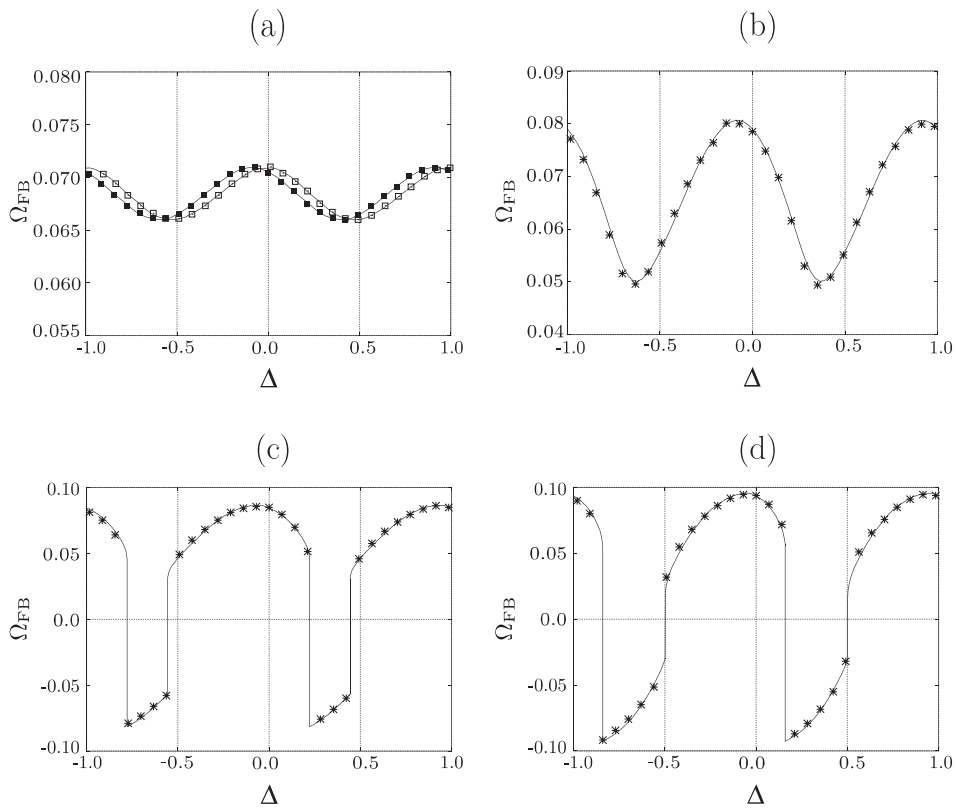

Figure 5. Relation between the frequency Ω_{FB} and the phase shift $\Delta = q_c\delta/2\pi$ for (a) $F = 0.0010$, (b) $F = 0.0057$, (c) $F = 0.0090$ and (d) $F = 0.0150$. In Figure (a), the simulation results are represented by the black squares, in comparison with the phase $\theta_2/2\pi$ (white squares) for the variable ϕ. In Figures (c)-(d) the results of simulations are represented by the symbols $*$, which should be compared with the theoretical results given in eqs. (39) and (40) (solid curves).

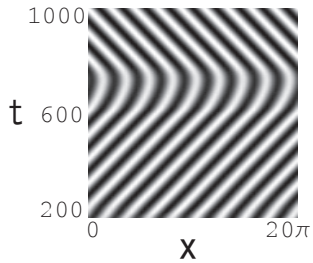

Figure 6. Space-time plot of the propagating wave. The gray scale indicates the magnitude of the variable ψ. The feedback forcing is changed at $t = 600$ from 0 to finite values $F = 0.009$ and $\Delta = 0.35$. Before this time, the wave propagates to the right. The feedback forcing eventually causes the propagation reversal.

It is evident from Figures 5(a)-(d) that the frequency depends sinusoidally on the shift for small values of the feedback strength F, with an amplitude that increases with F. In contrast to the case of external forcing, a stable wave exists both for $d\Omega_{FB}/d\Delta < 0$ and $d\Omega_{FB}/d\Delta > 0$. For $F < 0.0057$, the frequency Ω_{FB} is positive, which means that the wave propagates to the right under the feedback control. What is most noteworthy here is that the frequency jumps discontinuously at some value of Δ and changes its sign when F is large, as shown in Figures 5 (c) and (d). This reflects the reversal of the propagation direction of the wave train. A space-time plot of such reversal is displayed in Figure 6 for $F = 0.0090$ and $\Delta = 0.35$. Before the feedback control is turned on, at $t = 600$, the wave propagates to the right. However, after $t = 600$, the direction of propagating switches to the left.

Figures 7(a)-(d) display the propagating frequency Ω_{FB} as a function of the strength F for four values of the phase shift Δ. In Figure 7(a) it is seen that when the value of Δ is small, the frequency Ω_{FB} increases monotonically with the strength F. In fact, if the value Δ satisfies $d^2\Omega_{FB}/d\Delta^2 < 0$, then Ω_{FB} is an increasing function of F, since the amplitude of the sinusoidal variation of Ω_{FB} increases as a function of F, as can be seen in Figures 5 (a) and (b). When Δ exceeds a certain value, a discontinuity appears, as shown in Figures 7 (b) and (c). Then, for $\Delta > 0.5$, the frequency Ω_{FB} again becomes positive, as shown in Figures 5 (c) and (d), and, therefore, no discontinuity appears in Figure 7 (d) for $\Delta = 0.63$.

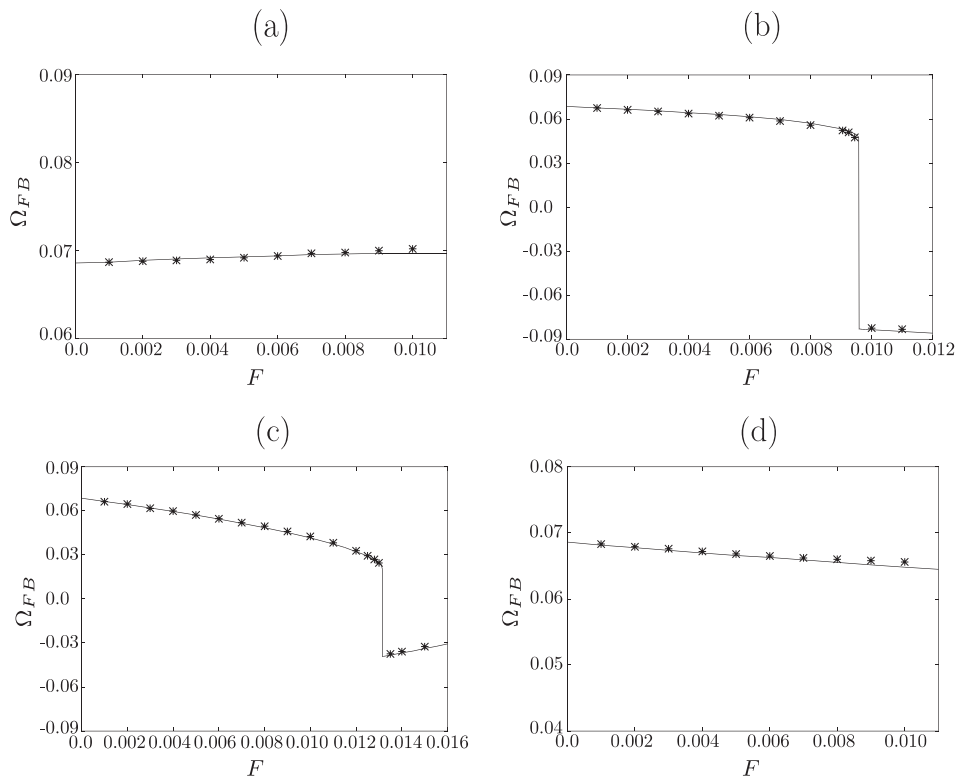

Figure 7. F-dependence of Ω_{FB} for $\Delta \approx 0.14$, (b) $\Delta \approx 0.21$, (c) $\Delta \approx 0.49$ and (d) $\Delta \approx 0.63$. The results of the simulations, represented by the symbols $*$, are compared with the theoretical results given by eqs. (39) and (40) (solid curves).

5. Phase Dynamics for Feedback Control

Now we formulate the phase dynamics for the case of feedback control [25]. The method here is similar to that for external forcing outlined in Section 3. In this case, we write

$$\psi = \psi_0 + \psi_1(t)\cos(q_c x - \omega_c t + \theta_1(t)), \tag{29}$$

$$\phi = \phi_0 + \phi_1(t)\cos(q_c x - \omega_c t + \theta_2(t)). \tag{30}$$

Substituting these into eqs. (27) and (28) and ignoring the higher harmonics,

we obtain

$$\omega_c - \frac{d\theta_1}{dt} = \frac{a_2\phi_1}{\psi_1}\sin(\theta_1-\theta_2) + F\sin(q_c\delta), \tag{31}$$

$$\omega_c - \frac{d\theta_2}{dt} = -\frac{b_1\psi_1}{\phi_1}\sin(\theta_1-\theta_2) + \frac{F\psi_1}{\phi_1}\sin\left(q_c\delta - (\theta_1-\theta_2)\right), \tag{32}$$

$$\frac{d\psi_1}{dt} = ({q_c}^4 + {q_c}^2(\tau-\tau_c))\psi_1 + a_1\psi_1 - \frac{3}{4}{q_c}^2\psi_1^3 + a_2\phi_1\cos(\theta_1-\theta_2) + F\psi_1\cos(q_c\delta), \tag{33}$$

$$\frac{d\phi_1}{dt} = b_1\psi_1\cos(\theta_1-\theta_2) + b_2\phi_1 + F\psi_1\cos\left(q_c\delta - (\theta_1-\theta_2)\right). \tag{34}$$

As in the case treated above, the amplitudes ψ_1 and ϕ_1 which evolve slowly in time are eliminated adiabatically by setting $d\psi_1/dt = d\phi_1/dt = 0$ and are obtained through a perturbation expansion with respect to ϵ. The zeroth order solutions, $\psi_1^{(0)}$ and $\phi_1^{(0)}$, are given by

$$\frac{3}{4}(\psi_1^{(0)})^2 = q_c^2 + \tau - \tau_c + \frac{1}{q_c^2}\left(a_1 - \frac{a_2b_1}{b_2}\left(\cos(\theta_1-\theta_2)\right)^2\right), \tag{35}$$

$$\phi_1^{(0)} = -\frac{b_1\psi_1^{(0)}}{b_2}\cos(\theta_1-\theta_2). \tag{36}$$

The first-order corrections, $\psi_1^{(1)}$ and $\phi_1^{(1)}$, are given by

$$\psi_1^{(1)} = \frac{2F}{3q_c^2\psi_1^{(0)}}[\cos(q_c\delta) - \frac{a_2}{b_2}\cos(q_c\delta-(\theta_1-\theta_2))\cos(\theta_1-\theta_2)], \tag{37}$$

$$\phi_1^{(1)} = \frac{\phi_1^{(0)}}{\psi_1^{(0)}}\psi_1^{(1)} - \frac{F\psi_1^{(0)}}{b_2}\cos\left(q_c\delta-(\theta_1-\theta_2)\right). \tag{38}$$

In this way, from eqs. (31), (32) and (35)-(38), we obtain

$$\omega_c - \frac{d\theta_1}{dt} = F\sin(q_c\delta) + a_2\frac{\phi_1^{(0)}}{\psi_1^{(0)}}\left(1 + \frac{\phi_1^{(1)}}{\phi_1^{(0)}} - \frac{\psi_1^{(1)}}{\psi_1^{(0)}}\right)\sin(\theta_1-\theta_2), \tag{39}$$

$$\omega_c - \frac{d\theta_2}{dt} = \frac{F\psi_1^{(0)}}{\phi_1^{(0)}}\sin(q_c\delta-(\theta_1-\theta_2)) - b_1\frac{\psi_1^{(0)}}{\phi_1^{(0)}}\left(1 + \frac{\psi_1^{(1)}}{\psi_1^{(0)}} - \frac{\phi_1^{(1)}}{\phi_1^{(0)}}\right)\sin(\theta_1-\theta_2). \tag{40}$$

We can show that the solutions of eqs. (39) and (40) in the limit $t \to \infty$

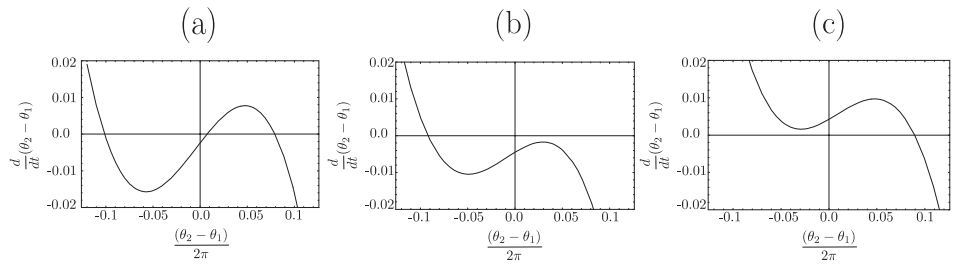

Figure 8. $d(\theta_2 - \theta_1)/dt$ as a function of $\theta_2 - \theta_1$ for $F = 0.009$ and for (a) $\Delta = 0.07$, (b) $\Delta = 0.35$ and (c) $\Delta = 0.63$.

take the form $\theta_1 = \omega t + c_1$ and $\theta_2 = \omega t + c_2$, where the constants ω and $c_2 - c_1$ are evaluated numerically. The frequency of the propagating wave under feedback control is given by

$$\Omega_{FB} = \omega_c - \omega. \tag{41}$$

The relation between Ω_{FB} and the phase shift variable defined by $\Delta = (q_c\delta)/(2\pi)$ is depicted by the solid curve in Figures 5 (a)-(d). The F-dependence is shown in Figures 7(a)-(d). It is found that these theoretical results agree almost completely with the simulations.

Next, we clarify the reason that Ω_{FB} becomes negative discontinuously as a function of Δ for large values of F. First, note that the right hand sides of eqs. (39) and (40) are functions of $\theta_2 - \theta_1$. Therefore, combining these two equations we obtain a closed equation for $\theta_2 - \theta_1$. Figures 8(a) - (c) plot $d(\theta_2 - \theta_1)/dt$ as functions of $\theta_2 - \theta_1$ for $\Delta = 0.07$, $\Delta = 0.35$ and $\Delta = 0.63$. For $\Delta = 0.07$, there are two stable and one unstable solutions, as shown in Figure 8 (a). Since we have chosen a wave propagating to the right, the phase difference $\theta_2 - \theta_1$ should be always positive. Therefore, the positive stable solution is approached asymptotically. However, when Δ is increased, the system becomes mono-stable, leaving only a stable negative solution, as shown in Figure 8(b). Hence, the value of $\omega_c - \omega$ exhibits a discontinuous jump when the transition from the bistability to the monostability occurs. If the value of Δ is increased further, the system again becomes bistable, and then eventually monostable once more, where, however, the stable solution for $\theta_2 - \theta_1$ is positive as in Figure 8(c).

6. Discussion

We have studied the dynamics of traveling waves under external and feedback control. We have found the following phenomena for the static external forcing. When external forcing is sufficiently strong the traveling waves are pinned. When the forcing is intermediate, trapped oscillations of wave trains are observed. We emphasize that the trapped oscillation of waves is a characteristic feature of traveling waves under external forcing, which never occurs in Turing patterns. We have performed theoretical analysis based on the phase equations.

The behavior of the propagation reversal under feedback control can be understood by the following general argument. First, we note that the equation for $\theta_2 - \theta_1$ takes the form

$$\frac{d(\theta_2 - \theta_1)}{dt} = a_0 F \sin(2\pi\Delta) + g(\theta_2 - \theta_1), \tag{42}$$

where a_0 and $g(x)$ contain F and Δ, as can be seen from eqs. (39) and (40). It is important to note that $g(x)$ is an odd function when the feedback control is absent (i.e., when $F = 0$). This is because the nonlinear dissipative wave considered here possesses a parity symmetry; that is, for every propagating wave in one direction, there is a corresponding wave propagating in the other direction obtained from the former through spatial reflection. This requires that eq. (42) should be invariant under the interchange of θ_1 and θ_2 and hence $g(x) = -g(-x)$ should take the following expansion

$$g(\theta_2 - \theta_1) = a_1(\theta_2 - \theta_1) - a_3(\theta_2 - \theta_1)^3 \tag{43}$$

for small values of $\theta_2 - \theta_1$ with positive coefficients a_1 and a_3. When $F \neq 0$, these coefficients generally depend on Δ. However as long as F is small, we can ignore such dependence. Then, eq. (42) with (43) reveals that the system is bistable when Δ or F is small. As Δ is increased, it becomes mono-stable with a negative solution for $a_0 < 0$, bistable and again mono-stable with a positive solution. This fact accounts for all of the results of the numerical simulations.

Although the present study starts with the specific model system, we believe that the results are quite general for traveling patterns independent of the details of the model equations. In fact, the coupled phase dynamics

given by eqs. (21) and (22) provides us with a general mechanism of trapped oscillations of domains under external force. The argument to derive eqs. eq. (42) with (43) for the reversal of the propagating direction is based only on the symmetry of the system without relying on any specific properties of the model system.

Acknowledgements and Dedication

We are grateful to H. Tokuda and V. S. Zykov for their collaboration of the present series of works. This work was supported in part by a Grant-in-Aid for the 21st Century COE "Center for Diversity and Universality in Physics" and a Grant-in-Aid for the priority area "Soft Matter Physics" both from the Ministry of Education, Culture, Sports, Science and Technology (MEXT) of Japan.

The author would like to dedicate this article to Professor Masayasu Mimura whose pioneering spirit towards Pattern Formation in Reaction-Diffusion Systems has always been inspired to him ever since he entered this profession.

References

1. Y. Nishiura, *Far-from-Equilibrium Dynamics*, American Math. Soc., 209, 2002.

2. M. Mimura, Dynamics of patterns and interfaces in some reaction-diffusion systems from chemical and biological viewpoints, *Methods and Appl. Analysis*, **8**(2001), 497-510 and the earlier references cited therein.

3. (eds) A. Pikovsky and Y. Maistrenko, *Synchronization: Theory and Application*, Kluwer, London, 2003.

4. Y. Tabe and H. Yokayama, Two-dimensional dynamic patterns in illuminated langmuir monolayers, *Langmuir* **11**, (1995) 4609-4613.

5. R. Reigada, F. Sagues and A. S. Mikhailov, Traveling waves and nonequilibrium stationary patterns in two-component reactive langmuir monolayers, *Phys. Rev. Lett.* **89**, (2002) 038301(1)-(4).

6. T. Okuzono, Y. Tabe and H. Yokayama, Generation, propagation, and switching of orientational waves in photoexcited liquil-crystalline monolayers, *Phys. Rev. E.* **69**(2004), 050701(1)-(4).

7. P. Coullet, Commensurate-Incommensurate Transition in Nonequilibrium Systems, *Phys. Rev. Lett.*, **56**(1986), 724-727.

8. C. W. Meyer, D. S. Cannell, G. Ahlers, J. B. Swift and P. C. Hohenberg, Patten competition in temporally modulated Rayleigh-Bénard convection, *Phys. Rev. Lett.*, **61**(1988), 947-950.

9. H. Riecke, J. D. Crawford and E. Knobloch, Time-modulated oscillatory convection, *Phys. Rev. Lett.*, **61**(1988), 1942-1945.

10. K. Martinez, A. L. Lin, R. Kharrazian, X. Sailer and H. L. Swinney, Resonance in periodically inhibited reaction-diffusion systems, *Physica D*, **168-169**(2002), 1-9.

11. V. K. Vanag, A. M. Zhabotinsky and I. R. Epstein, Oscillatory Clusters in the Periodically Illuminated, Spatially Extended Belousov-Zhabotinsky Reaction, *Phys. Rev. Lett.*, **86** (2001), 552-555.

12. S. Rüdiger, D. G. Míguez, A. P. Muñuzuri, F. Sagués, and J. Casademunt, Dynamics of Turing Patterns under Spatiotemporal Forcing, *Phys. Rev. Lett.*, **90**(2003), 128301(1)-(4).

13. A. S. Mikhailov and K. Showalter, Control of waves, patterns and turbulence in chemical systems, *Physics Reports* **425** (2006), 79-194.

14. V. S. Zykov, G. Bordiougov, H. Brandtstädter, I. Gerdes, and H. Engel, Periodic forcing and feedback control of nonlinear lumped oscillators and meandering spiral waves, *Phys. Rev. E* **68** (2003), 016214(1)-(14).

15. W. Vance and J. Ross, Entrainment, phase resetting, and quenching of chemical oscillations, *J. Chem. Phys.*, **103** (1995), 2472-2481.

16. L. Glass and W. Zh. Zeng, Complex Bifurcations and Chaos in Simple Theoretical Models of Cardiac Oscillations, *Annals of New York Academy Sciences*, **591** (1990), 316-327.

17. C. Utzny, W. Zimmermann, and M. Bär, Resonant spatio-temporal forcing of oscillatory media, *Europhys. Lett.*, **57** (2002), 113-119.

18. M. Henriot, J. Burguete, and R. Ribotta, Entrainment of a spatially extended nonlinear structure under selective forcing, *Phys. Rev. Lett.*, **91** (2003), 104501(1)-(4).

19. D. G. Miguez, E. M. Nicola, A. P. Munuzuri, J. Casademunt, F. Sagués, and L. Kramer, Traveling-stripe forcing generates hexagonal patterns, *Phys. Rev. Lett.*, **93** (2004), 048303(1)-(4).

20. S. Rüdiger, E. M. Nicola, J. Casademunt and L. Kramer, Theory of pattern forming systems under traveling-wave forcing, *Physics Report*, **447** (2007), 73-111.

21. S. Zykov, V. S. Zykov, and V. Davydov, Spiral wave dynamics under traveling-wave modulation of excitable media, *Europhys. Lett.*, **73** (2006), 335-341.

22. N. J. Wu, H. Zhang, H.-P. Ying, Z. Cao, and G. Hu, Suppression of Winfree turbulence under weak spatiotemporal perturbation, *Phys. Rev. E*, **73** (2006), R060901(1)-(4).

23. T. Ohta and H. Tokuda, Dynamics of traveling waves under spatiotemporal forcing, *Phys. Rev. E*, **72**(2005), 046216(1)-(8).

24. H. Tokuda and T. Ohta, Entrainment and modulation of nonlinear dissipative waves under external forcing, *J. Phys. Soc. Jpn*, **75** (2006), 064005(1)-(9).

25. H. Tokuda, V. S. Zykov and T. Ohta, External forcing and feedback control of nonlinear dissipative waves, *Phys. Rev. E*, **75**(2007), 066203(1)-(11).

26. T. Okuzono and T. Ohta, Self-propulsion of cellular structures in chemically reacting mixtures, *Phys. Rev. E*, **64**(2001), R045201(1)-(4).

27. T. Okuzono and T. Ohta, Traveling waves in phase-separating reactive mixtures, *Phys. Rev. E*, **67**(2003), 056211(1)-(10).

28. S. Sugiura, T. Okuzono, and T. Ohta, Time-modulated oscillatory structures in phase-separating reactive mixtures, *Phys. Rev. E*, **66**(2002), 066216(1)-(7).

Department of Physics, Kyoto University, Kyoto, 606-8502, Japan.

E-mail: takao@scphys.kyoto-u.ac.jp